Noise-aided computation within a synthetic gene network through morphable and robust logic gates

Anna Dari,[1] Behnam Kia,[1,2] Xiao Wang,[1] Adi R. Bulsara,[3] and William Ditto[1]
[1]*School of Biological and Health Systems Engineering, Arizona State University, Tempe, Arizona 85287-9709, USA*
[2]*School of Electrical, Computer and Energy Engineering, Arizona State University, Tempe, Arizona 85287-5706, USA*
[3]*SPAWAR Pacific Code 71000, San Diego, California 92152-5001, USA*
(Received 26 May 2010; revised manuscript received 28 December 2010; published 11 April 2011)

An important goal for synthetic biology is to build robust and tunable genetic regulatory networks that are capable of performing assigned operations, usually in the presence of noise. In this work, a synthetic gene network derived from the bacteriophage λ underpins a reconfigurable logic gate wherein we exploit noise and nonlinearity through the application of the logical stochastic resonance paradigm. This *biological logic gate* can emulate or "morph" the AND and OR operations through varying internal system parameters in a noisy background. Such genetic circuits can afford intriguing possibilities in the realization of engineered genetic networks in which the actual function of the gate can be changed *after* the network has been built, via an external control parameter. In this article, the full system characterization is reported, with the logic gate performance studied in the presence of external and internal noise. The robustness of the gate, to noise, is studied and illustrated through numerical simulations.

DOI: 10.1103/PhysRevE.83.041909 PACS number(s): 87.18.Cf

I. INTRODUCTION

The goal of synthetic biology is to extend or modify the behavior of organisms as well as engineer them to perform new tasks [1,2]. Conventional genetic engineering approaches for solving complex problems typically focus on single genes. Moreover, the experimental progress of recent years has made the design and implementation of genetic regulatory networks (GRNs) amenable to quantitative analysis. A GRN can be visualized as composed of subsets of simpler components (modules), interconnected trough input and output signals (analogous to electrical circuits [3]). In the same way that electrical engineers construct circuits, genetic network engineers make use of the biological equivalents of inverters and transistors to manipulate living organisms by connecting these modules into GRNs that can control cellular functions [4,5].

There are two important reasons for constructing synthetic networks: (i) the reduction of the cell complexity (the inherently reductionist approach of decoupling a simple network from its native and often complex biological setting can yield valuable information regarding evolutionary design principles [3]) and (ii) the manipulation and monitoring of single genes can, in the future, afford the possibility of building larger functional systems [6].

One of the immediate strategies in the (relatively new) field of synthetic biology has been to develop a toolbox [7,8] of well-characterized genetic circuits and devices [2]. Recent efforts have yielded an ever-growing number of synthetic biological devices with varied functional capabilities, including memory devices [9], linearizer gene circuit [10], switches [5,8,11], oscillators [12,13], amplifiers [14,15], and time-delayed circuits [16,17]. The implementation of all these biological circuits is possible through the regulation of cellular functions at the gene level. To achieve this task, a theoretical modeling of the gene expression dynamics is required. For a complete analysis, two important ingredients cannot be removed and have to be considered: nonlinearity and random fluctuations. It is often assumed that noise has a negative influence on cellular processes and should be avoided when engineering genetic circuits that require exquisite control; this has been accomplished via, e.g., synthetic transcriptional cascades that attenuate noise under specific conditions [10,18,19]. In general, however, the delicate interplay between noise and nonlinearity should be well characterized for an optimal understanding/prediction of the system performance. This is particularly true in natural systems wherein the noise is, quite often, the "signal" (rather than simply a laboratory curiousity) or the driving force that lets the system change its state [20]. As one might expect, depending on the goal, external noise and fluctuations at the genetic level can either be undesirable or useful. Importantly, genetic circuits (whether naturally occurring or synthesized) have to be reliable, robust, and predictable; this is best achieved through exploiting the interaction between noise and nonlinearity with a view to enhancing performance. A good example of this is the (now well-known) scenario of stochastic resonance (SR): an optimal range of noise intensity can enhance the system response to weak input signals [21–23].

Noise originates from many sources and is, for simplicity, divided in two classes: *internal* and *external*. The first one includes fluctuations in the gene expression (transcription, translation, and degradation), cell cycle variations, and differences in the concentrations of metabolites. Its magnitude is related to the system size, and its origin is often thermal [24]. External noise usually originates from extrinsic environmental variations [25].

In this work, we propose and study the possibility of implementing a *biological logic gate* that can emulate and "morph" (i.e., switch between) the AND and OR operations, by exploiting noise. In particular, we show how the desired output signal occurs consistently and robustly in an *optimal* range of noise values. The realization of this biological system is obtained through the application of logical stochastic resonance (LSR) whose general principle will be detailed in the following section. The intriguing novelty of LSR in a GRN is to allow a single module to be used for many different applications via adjusting the network parameters to obtain

specific functionalities. We are thus led to study the realization of a biological logic gate with the requirement of maximal flexibility. As explained in this work, with LSR we can define a large range of values that can be adjusted to switch the gate between the AND and OR configurations and be robust to noise. Thus, we are proposing a *synthesized* GRN that can perform the logic functions (e.g., AND/OR), can be used in different environments, and *can change its behavior after it has been engineered*.

The core of this work is to demonstrate, through simulations, the real possibility of implementing LSR in a GRN. This task has been achieved by introducing the Langevin equation for the repressor protein concentration. We show a robust logic gate performance in a noisy environment, and we test the possibility of morphing between AND and OR gates. In order to theoretically demonstrate the validity of this idea in a GRN we study the system, first, in the presence of an additive noise term (for modeling an external noise source) and, second, in the presence of a multiplicative noise term (for modeling the internal noise). We begin with a review of the LSR paradigm [26]. Then, in Sec. III after introducing the basic concepts of gene expression, we study in detail a single GRN: a synthetic gene network derived from the bacteriophage λ [4,27–29]. In particular, we focus on the characterization of the dynamics of the λ repressor protein concentration. From the analysis of the biochemical reactions we write, as our starting point, the deterministic differential equation that displays the bistability of the GRN in a certain parameter regime. The complexity of this system and the allowed range of parameter values, necessitates our introducing a new version of the LSR paradigm (see Sec. IV). The nonlinear dynamics of the GRN, in the presence of the internal and external sources, are studied in the remainder of the article.

II. LOGICAL STOCHASTIC RESONANCE: THE BASIC PRINCIPLE

For completeness, this section provides an outline of the main features that characterize LSR; this paradigm was, recently, put forward by Murali *et al*. [26,30,31]. First, consider the basic functioning of a logic gate. Its logic input N_i (where i is the input number, in this case 1 and 2) can be either 0 or 1. We then have a four-distinct-logic input set $(N_1,N_2) = (0,0),(0,1),(1,0)$, and $(1,1)$; since in this work the two inputs enter in the system equation as the sum $N_1 + N_2 = N$, the input set reduces to three combinations, with $(0,1)$ and $(1,0)$ yielding the same N. The output of the logic gate can be either 0 or 1. In summary, for a given set of inputs (N_1,N_2), we obtain a *logical* output in accordance with the truth table (Table I).

The generalized truth functions (row 4 of Table I) for the case of an arbitrary input set (x_1,x_2) with $0 \leqslant x_{1,2} \leqslant 1$ are particularly, relevant in the presence of input noise and in cases where we do not digitize the input. We note that the first three rows of Table I directly follow from the general case. The generalized logic function $\mathrm{NAND}(x_1,x_2)$ can be obtained from $\mathrm{NOR}(x_1,x_2)$ by simple deduction: $\mathrm{NAND}(x_1,x_2) = \mathrm{NOT}[\mathrm{AND}(x_1,x_2)] = 1 - \mathrm{AND}(x_1,x_2) = 1 - \min(x_1,x_2) = 1 - [1 - \max(1 - x_1,1 - x_2)] = \max(1 - x_1,1 - x_2)$, where the penultimate step is a direct consequence of deMorgan's Law (for all real numbers), and we have invoked the definition $\mathrm{NOT}(x) = 1 - x$. A similar derivation leads to the logic function $\mathrm{NOR}(x_1,x_2) = \min(1 - x_1,1 - x_2)$.

We consider now a stochastic nonlinear system:

$$\dot{x} = F(x,a,b,\dots) + N + D_n\xi(t), \tag{1}$$

where a and b are two possible parameters that characterize the generic nonlinear function F given in the deterministic system by the negative gradient of a potential function with two stable attractors (in this article we consider fixed point attractors corresponding to a bistable potential). The second term in Eq. (1) is the input signal that can assume the values reported in Table I. Finally, $\xi(t)$ represents additive zero-mean Gaussian noise with unit variance and intensity parameter D_n (typically, D_n would be the standard deviation). We assume that random fluctuations have a correlation time scale smaller than any other reaction time scale in the system, so the noise can be taken to be δ correlated [i.e., $\langle\xi(t)\xi(t')\rangle = \delta(t - t')$]. For the moment we do not consider the case of state-dependent (or multiplicative) noise; this will be addressed later in this work.

In a system underpinned by dynamics of the form (1), the LSR paradigm affords the possibility to exploit noise in order to get a desired logic gate performance with almost unit probability, i.e., the operation is rendered quite reliable even in the noisy environment. Indeed, Murali *et al*. found that, in an optimal range of noise intensity values, the performance of the system is optimized and its output is the logical combination of the two input signals. Thus, the LSR paradigm underpins the realization of morphable and reliable logic gates in the presence of noise: changing parameters such as a and b, or applying a controllable dc asymmetrizing system to the dynamics Eq. (1), one can switch from the AND to the OR gate. Hence, LSR is a practical and reasonable paradigm to be applied in computational devices wherein the noise-floor cannot be suppressed [30].

TABLE I. Truth table of the fundamental OR, AND, NOR, and NAND logic operations. Since the inputs are encoded as $N = N_1 + N_2$, the input set reduces to three terms. For completeness, we have shown the truth functions for a general (i.e., "fuzzy") set of inputs with $0 \leqslant x_{1,2} \leqslant 1$.

Input set (N_1,N_2)	OR	AND	NOR	NAND
(0,0)	0	0	1	1
(0,1)/(1,0)	1	0	0	1
(1,1)	1	1	0	0
(x_1,x_2)	$\max(x_1,x_2)$	$\min(x_1,x_2)$	$\min(1 - x_1,1 - x_2)$	$\max(1 - x_1,1 - x_2)$

III. BISTABILITY IN A SINGLE-GENE NETWORK

The complex functions of a living cell are carried out through the concerted activity of many genes and gene products. This activity is often coordinated by the organization of the genome into regulatory networks. In this section, we will recover the function F [in Eq. (1)] that characterizes the synthetic gene network under consideration, in the deterministic ($D_n = 0$) regime.

For completeness we introduce, in this section, the basic concepts of gene expression dynamics [32,33]. The DNA in genomes does not direct protein synthesis itself but instead uses RNA polymerase as an intermediary. In particular, the RNA polymerase will bind in a specific segment of the DNA, known as the *promoter region*. An mRNA is then produced when the RNA polymerase molecule initiates transcription at the promoter level, synthesizes the RNA by chain elongation, stops transcription at a terminator, and releases both the DNA template and the mRNA molecule. Therefore, one can speak of the promoter as the most important point of control of a specific gene expression. Afterward, mRNA is decoded by the ribosome to produce a specific amino acid chain that later folds into an active protein. Among all proteins, gene regulatory proteins switch the transcription of individual genes on and off. They usually bind the DNA in specific regions close to the RNA polymerase start site and, depending on the nature of the regulatory protein and the location of its binding site relative to the start site, either activate or repress transcription. The time and the place that each gene is transcribed, as well as its rate of transcription under different conditions, are determined by the spectrum of gene regulatory proteins that bind the regulatory region of the gene. These reactions are controlled by feedback loops that arise when the translated protein is capable of interacting with the promoter(s) of its own genes and of other genes. Feedback can occur in the positive (activation) or negative (repression) sense [7,10,13,19]. Typically, we can find proteins in a homodimer or heterodimer form that is responsible for the presence of a nonlinearity in genetic networks.

In this work we adopt an engineering approach in describing the design of a synthetic network present in the virus bacteriophage λ. Because of the complexity of the whole system, we have focused our study on a solitary gene network (or autoregulatory gene network) [29,34]. This restriction has two advantages. In principle it affords the possibility of better prediction of the system dynamics via a mathematical formulation and, thus, an understanding of the cellular behavior. Second, a deeper knowledge of the simple autoregulatory network taking noise into account can lead to several applications which exploit the noise, such as LSR.

Bacteria and their temperate phages, e.g., *Escherichia coli (E. coli)* and λ, exist in symbiotic relationships. After the λ phage infects the bacteria, the evolution of the λ phage proceeds down one of the two pathways: lytic or lysogenic [4,27,28]. Each pathway depends on the controlled sequential synthesis and subsequent activity of λ-encoded proteins. Lytic infection by the phage λ results in the release of hundreds of new phages per infected cell. The minimum set of events in the growth cycle is, therefore, DNA replication, phage particle synthesis, and cell lysis. The creation of new phage progeny can, then, infect other bacteria. In the lysogenous pathway, the temperate phage induces a change in the phenotype of the infected bacteria through the incorporation of the phage DNA into the host genome. The newly integrated genetic material, called a prophage, can be transmitted to daughter cells at each subsequent cell division, and a later event (such as UV radiation) can release it, causing proliferation of new phages via the lytic cycle.

The key section of the decision between one of the two pathways lies in the right operator region (O_R), in which three DNA-binding sites are recognized by two phage-encoded regulatory proteins: the λ repressor protein (also called CI) and Cro. O_{R1}, O_{R2} and O_{R3}, the three operator sites, overlap the promoter regions of the genes that encode these same proteins: the P_{RM} (where RM is repressor maintenance) promoter controls the expression of cI and the P_R (where R is repressor) promoter controls the expression of cro. The pattern of CI/Cro binding to the three operator sites determines whether the lysogenic or lytic pathway will be followed [27]. Hence, the bacteriophage λ displays bistability in the choice of one of two pathways, with the characteristics of its stable attractors adjustable by externally changing the system parameters.

Here we focus our study only on the regulation of the P_{RM} operator region in a DNA plasmid: an autoregulatory network (see Fig. 1) that shows a binary decision making through a positive feedback loop [29,35,36]. In this feedback loop, O_{R1}, O_{R2} activate transcription, while O_{R3} represses transcription. The repressor protein CI binds to the DNA in one of the three O_{Ri} sites. CI is expressed by the gene cI and subsequently dimerizes. Depending on the binding affinities, binding happens as follows: the dimer first binds to the O_{R1} site, then to O_{R2} (where a downstream transcription is enhanced) and, finally, to O_{R3} (that effectively turns off the protein production) [37,38].

For a complete comprehension of the autoregulatory gene network described above, we have developed a quantitative model. Consider, first, the biochemical reactions that characterize our network. These reactions are very well understood [27,38] and are categorized depending on the order of the rate

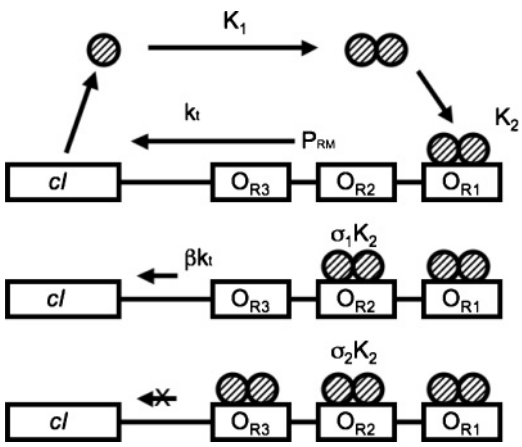

FIG. 1. Autoregulatory gene network: the promoter region contains three operator sites (O_{R1}, O_{R2}, and O_{R3}). The cI gene expresses the λ repressor protein, which in turn dimerizes and then binds to the operator sites.

at which they occur. The ones that have a rate constant of the order of seconds (fast reactions) are considered to be at equilibrium; such reactions are referred to as multimerization (in this article we will consider only dimerization) or as the binding between the dimer and the operator site. The other reactions with rates of the order of minutes are considered slow reactions.

Here we list the fast reactions used to describe our model:

$$\begin{aligned} X + X &\rightleftharpoons X_2, \quad D + X_2 \rightleftharpoons D_1, \\ D_1 + X_2 &\rightleftharpoons D_2D_1, \quad D_2D_1 + X_2 \rightleftharpoons D_3D_2D_1, \end{aligned} \tag{2}$$

where X, X_2, D, and D_i are the repressor monomer, the repressor dimer, the DNA promoter region, and the dimer binding to the O_{Ri} operator site, respectively. Moreover, each fast reaction is characterized by an equilibrium constant ($K_i = k_i/k_{-i}$, where k_i and k_{-i} are the rate constant): K_1, K_2, $K_3 = \sigma_1 K_2$, and $K_4 = \sigma_2 K_2$, in order from the first to the fourth equation in (2). σ_1 and σ_2 represent the binding strengths relative to the dimer-O_{R1} strength.

In addition to (2), we have to consider the slow reactions: transcription, degradation, and dilution. We assume that dilution due to cell growth is, likely, slower than monomer degradation but comparable (in time scale) to transcription. These reactions are irreversible. In particular, if one repressor dimer binds to the first right operator site (O_{R1}), transcription proceeds at the basal rate. Moreover, an amplification of transcription occurs when a subsequent repressor dimer binds to O_{R2}: the binding affinity to the RNA polymerase is increased of a factor β. We write the reactions governing these processes as

$$\begin{aligned} D_1 + P \rightarrow D_1 + P + nX, \quad D_2D_1 + P \rightarrow D_2D_1 + P + nX \\ X \rightarrow \phi, \quad X_2 \rightarrow \phi, \end{aligned} \tag{3}$$

where each of the listed reactions in (3) are characterized by a rate constant: k_t (for transcription rate while one dimer is bound to the O_{R1} operator site), βk_t (for transcription enhanced by a factor β), k_x (for degradation), and k_y (for dilution). P denotes the concentration of RNA polymerase, and n is the number of repressor proteins per mRNA transcript.

While the reaction rates are embodied by rate laws [as Eqs. (2) and (3)], the biochemical dynamics can be described with differential equations. If we consider high copy-number plasmids, the dynamics in this gene network can be described by the evolution of the λ repressor concentration in the monomer and dimer form as follows:

$$\begin{aligned} \dot{x} &= -2k_1x^2 + 2k_{-1}x_2 + nk_t p_0(d_1 + \beta d_2) - k_x x + \epsilon d_0 \\ \dot{x_2} &= k_1x^2 - k_{-1}x_2 - k_y x_2, \end{aligned} \tag{4}$$

where we assume that the concentration of the RNA polymerase p_0 to be constant and ϵ is the basal expression rate. In particular, the concentrations in our system have been defined as $x = [X]$, $x_2 = [X_2]$, $d_0 = [D]$, $d_1 = [D_1]$, $d_2 = [D_2D_1]$, and $d_3 = [D_3D_2D_1]$. We next simplify the first equation in (4) as follows:

$$\begin{aligned} \dot{x} &= -2k_1x^2 + 2k_{-1}x_2 + nk_t p_0 d_1 + nk_t p_0 \beta d_2 - k_x x + \epsilon d_0 \\ &= -2k_1x^2 + 2k_{-1}x_2 + (nk_t p_0 - \epsilon + \epsilon)d_1 \\ &\quad + (nk_t p_0 \beta - \epsilon + \epsilon)d_2 - k_x x + \epsilon d_0 \\ &= -2k_1x^2 + 2k_{-1}x_2 + (nk_t p_0 - \epsilon)d_1 + (nk_t p_0 \beta - \epsilon) \\ &\quad \times d_2 - k_x x + \epsilon(d_0 + d_1 + d_2 + d_3) - \epsilon d_3. \end{aligned} \tag{5}$$

Moreover, for the fast reactions in Eq. (2), that are considered at equilibrium, the mathematical formulation is:

$$\begin{aligned} x_2 = K_1x^2, \quad d_1 = K_1K_2d_0x^2, \quad d_2 = \sigma_1(K_1K_2)^2 d_0x^4, \\ d_3 = \sigma_1\sigma_2(K_1K_2)^3 d_0x^6. \end{aligned} \tag{6}$$

In addition, we also consider to be constant the total concentration of DNA promoter sites, d_T (where the subscript T refers to total); this can be written as:

$$d_T = d_0 + d_1 + d_2 + d_3 \tag{7}$$

and at the same time $\epsilon d_T = r$ is constant. We can now explicitly calculate d_0 from (6) and (7):

$$d_0 = \frac{d_T}{1 + K_1K_2x^2 + \sigma_1(K_1K_2)^2x^4 + \sigma_1\sigma_2(K_1K_2)^3x^6}. \tag{8}$$

The dimerization reactions are the faster reactions; this has allowed us to simplify the system. Under these assumptions, the first two terms of both equations in (4) will cancel. However, this will leave only one negative term on the right-hand side of the second equation. To accurately model the evolution of the chemical species x, we define the variable $x_{\text{tot}} = x + 2x_2$; this represents the total number of biomolecules in the system, either dimer (where two molecules are consumed) or monomer (where one molecule is consumed). Then, Eqs. (5)–(8) can be reorganized as:

$$\dot{x}_{\text{tot}} = \dot{x} + 2\dot{x_2} = \frac{d_T(K_1K_2(nk_t p_0 - \epsilon)x^2 + (nk_t p_0 \beta - \epsilon)(K_1K_2)^2\sigma_1x^4 - \epsilon\sigma_1\sigma_2(K_1K_2)^3x^6}{1 + K_1K_2x^2 + \sigma_1(K_1K_2)^2x^4 + \sigma_1\sigma_2(K_1K_2)^3x^6} + r - k_x x - 2K_1k_y x^2, \tag{9}$$

To work in terms of the repressor concentration in the monomer form, we can, explicitly, write the left-hand side of Eq. (9):

$$\dot{x}_{tot} = \dot{x} + 2\dot{x_2} = \dot{x} + 4K_1x\dot{x} = (1 + 4K_1x)\dot{x}, \tag{10}$$

where the relation between x and x_2 has been shown in Eq. (6). We can now divide by $(1 + 4K_1x)$ on the left- and right-hand sides of Eq. (9). Further, without loss of generality, we can define the dimensionless variables $\tilde{x} = x\sqrt{K_1K_2}$ and $\tilde{t} = trK_2/4$. Under these assumptions, and after some calculations, we obtain the dimensionless equation (we have suppressed the overbar on x and t):

$$\dot{x} = \frac{(\alpha - 1)x^2 + \sigma_1(\alpha\beta - 1)x^4 - \sigma_1\sigma_2x^6}{(\tau + x)(1 + x^2 + \sigma_1x^4 + \sigma_1\sigma_2x^6)} + \frac{1 - \gamma x - \gamma_y x^2}{\tau + x}, \tag{11}$$

TABLE II. Parameters relevant to this autoregulatory gene network.

Parameter value	Meaning
$\beta = 11$	Degree of transcriptional activation
$K_1 = 5.0 \times 10^7\ \mathrm{M}^{-1}$	Equilibrium constant for dimerization
$K_2 = 0.33 \times 10^7\ \mathrm{M}^{-1}$	Equilibrium constant for dimer-O_R reaction
$\sigma_1 = 2$	Binding affinity for the dimer to O_{R2} relative to O_{R1}
$\sigma_2 = 0.08$	Binding affinity for the dimer to O_{R3} relative to O_{R1}

where we introduce the dimensionless parameters $\alpha = nk_t p_0 d_T/r$, $\gamma = k_x/(\sqrt{K_1 K_2}r)$, $\gamma_y = 2k_y/(rK_2)$, $\tau = \sqrt{K_1 K_2}/4K_1$. In Eq. (11) the first term on the right-hand side is related to the expression of the repressor protein because of transcription. The x^2, x^4, and x^6 terms are due to the dimerization of the λ repressor and the subsequent binding to the operator sites. The x^6 term represents, for example, the occupation of all three operator sites. The second term includes the basal expression rate (while there is no binding to the DNA), the degradation and the dilution that have the role of reducing the protein concentration in the cell. Moreover, we set (and retain throughout this work) values for the constants that are relevant to this autoregulatory network as in Refs. [34,39–41]. The whole list of constants is detailed in in Table II. Selecting them ensures that our calculations are always within the space of *biologically accessible* parameter ranges.

Equation (11) is the deterministic dynamical model that we will consider throughout this work; its right-hand side is the function F in Eq. (1), and α and γ are particular examples of the listed parameters (a and $b, \ldots$) in Eq. (1). Although it seems complex and contains several nonlinear terms, the potential function characterizing the system is bistable in a particular range of parameters, as will be shown below. In other words, the repressor concentration can assume (with a high probability) two favorable values (the minima in the potential function) that correspond to lytic or lysogenic pathways.

Before going further, we must interject an important comment. The model derived in this section is not the most general model for the λ phage switch; that distinction belongs to the model of Morelli *et al*. [42]. However, for the purpose of illustrating the LSR effect (albeit through a modified paradigm that we introduce in the next section) and demonstrating the realizability of the fundamental logic operations in a biological switch, the model of this section is quite adequate.

IV. A MODIFIED VERSION OF LSR

In this work, we propose a modified version of the LSR paradigm, via a manipulation of the conventional principle reported in Sec. II. The modification is necessary because of the unique (highly asymmetric) structure of the potential energy function that characterizes this system; the conventional LSR paradigm yields somewhat suboptimal performance in this case. In addition, we wish to confine our calculations to the space of biologically relevant parameters; these parameters include the system (additive or multiplicative) noise parameters. We introduce two significant changes.

First, we have characterized LSR in an autoregulatory network not only in the additive noise regime (as in Eq. (1) and in Ref. [26]) but also in the multiplicative noise case. Therefore the dynamical equation takes the more general form:

$$\dot{x} = F[x,a,b,\ldots,D_m\eta(t)] + D_n\xi(t), \tag{12}$$

where $\eta(t)$ is a multiplicative zero-mean Gaussian noise with unit variance and intensity parameter D_m. In general, this noise can affect one or more parameters (listed with symbols a and b above) and, consequently, the system "energy landscape.' While the multiplicative noise intensity D_m differs from zero, the term F will be a stochastic nonlinear function. In addition, we have to make clear that, for a concrete application of LSR to a biological model, the set of logic gate inputs are not added as in Eq. (1) but are, instead, implemented through the parameter values such as a, b, etc. [in the specific biological system of this work, the parameters are α and γ, see Eq. (11)].

Second, we tried to enhance the logic gate performance and to enlarge the noise intensity range where it is possible to implement LSR in this particular gene network. This necessity is, largely, connected to the biological model we are using: it does not yield enough dynamical range to successfully implement the (conventional) LSR paradigm [26]. Since, in Ref. [26], the authors were working with abstract mathematical models, they had full control over the system dynamics, in particular the depth and width of the potential wells; hence, they were able to adjust the dynamical system so it neatly fit the requirements of (conventional) LSR: the system parameters (a, $b, \ldots$) were chosen to provide well-defined bistability for all the distinct logic input sets given in the truth table. To illustrate this point, we have plotted, in Fig. 2, the bifurcation diagram for the general function F in Eq. (11) versus α (that is one of the two parameters we will use to implement the logic gates); in this case, we obtain bistability with a concommitant reliable implementation of the conventional LSR paradigm for α over 10.

The new idea is to choose the parameters of the model so the undesired well (almost) disappears and to take advantage of stochastic resonance for the cases where one cannot, simply, remove the unwanted well from the system potential function,

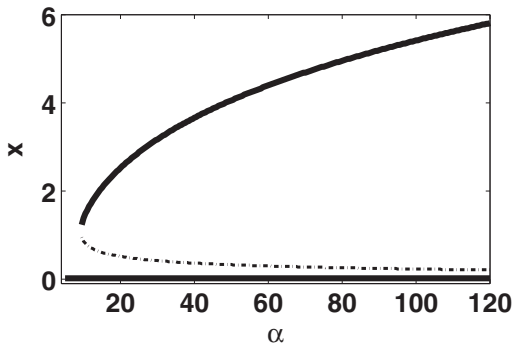

FIG. 2. Bifurcation diagram of the dimensionless protein concentration x in Eq. (11) versus α. The bistable behavior is visible for a fixed value of $\gamma = 50$.

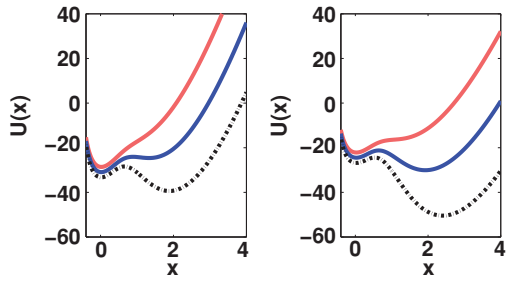

FIG. 3. (Color online) Potential functions for different data inputs for the AND gate (left panels) and the OR gate (right panels), using the modified version of the LSR paradigm. The red (upper) curve represents the (0,0) case, the blue (central) curve represents the (0,1)/(1,0) cases, and the black (lower) curve is for the (1,1) case. Values in the accessible parameter range, related to the most robust configuration (see text), have been chosen.

$U(x)$. This second case usually happens when the inputs are (0,1)/(1,0). With this proposed model we simply want to take into account all the range of the parameter values that represents all the possible biological configurations, without restricting our study to the bistable region. Put differently, there is the possibility that the (0,0) or (1,1) cases can be realized when $U(x)$ is monostable. In Fig. 3, we have plotted the potential function $U(x)$ for the AND and OR gates and for the three input sets. The red curve, that shows the (0,0) case, is in the monostable configuration.

Through the parameter γ, then, we can deepen either well in $U(x)$, selectively, to switch from one logic gate to the other; hence with the appropriate amount of noise, trajectories will switch to the deeper well and remain there, giving rise a better performance. The modified LSR paradigm will work in a broader range of parameters. Considering Fig. 2, the possible working range can now be extended to α higher than 5.

V. ADDITIVE NOISE

Since the early 2000s, the study of cells and their inner dynamics has revealed the presence of noise as a relevant element for the complete characterization and knowledge of the system itself [43,44]. In this section we will focus only on the *external* noise source. If we consider our variable x to be the repressor protein concentration as detailed in Sec. III, we can characterize the noise as random alterations (i.e. fluctuations) of the "background" repressor production. For the construction of our stochastic model, we suppose that these random fluctuations will affect the basal production term r. Moreover, we consider that such external effects will be small and, therefore, can be treated as a random additive perturbation to the deterministic dynamics [see Eq. (11)]:

$$\dot{x} = \frac{(\alpha-1)x^2 + \sigma_1(\alpha\beta-1)x^4 - \sigma_1\sigma_2 x^6}{(\tau+x)(1+x^2+\sigma_1 x^4+\sigma_1\sigma_2 x^6)} + \frac{1-\gamma x-\gamma_y x^2}{\tau+x} + D_n\xi(t), \quad (13)$$

where $\xi(t)$ is the additive (*external*) zero-mean Gaussian noise [$\langle\xi(t)\rangle = 0$], and $\langle\xi(t)\xi(t')\rangle = \delta(t-t')$, with D_n being related to the noise standard deviation parameter (as already introduced in Sec. II).

From Eq. (13) we can get the corresponding Fokker-Planck equation [45] for $P(x,t)$, the probability of finding the system in a state with concentration x at the time t:

$$\frac{\partial P(x,t)}{\partial t} = -\frac{\partial}{\partial x}[F(x)P(x,t)] + D_n\frac{\partial^2}{\partial x^2}P(x,t), \quad (14)$$

where F is the nonlinear function in the right-hand side of Eq. (11). Then the steady-state probability density function is given as:

$$P_S(x) = N_{\text{add}}\exp\left[-\frac{U(x)}{D_n}\right], \quad (15)$$

where we obtain the potential shape $U(x)$ from the definition of $F(x) = -\partial U(x)/\partial x$; the "particle-in-potential" analogy leads us to view $U(x)$ as an "energy landscape," wherein $x(t)$ is the position of a hypothetical "particle" following the stochastic dynamics (13). $U(x)$ is bistable in a parameter range (see Sec. IV) and the concentration x has fixed values at the minima of $U(x)$. N_{add} is the normalization constant resulting from making the integral of $P_S(x)$ over all x equal to unity. In Fig. 3, we have plotted the potential $U(x)$ for a particular combination of parameter values. We can notice the (somewhat dramatic) asymmetry of the potential function: the left and right energy barrier heights differ, together with the curvatures in the bottom of the potential wells.

In the presence of noise the system can, with different probabilities, span all the allowed x values that are biologically meaningful. If the noise intensity is very small compared to the two energy barriers, the system mainly remains confined in one of the two potential wells and randomly moves around in the minimum (i.e., *intra*well motion). A larger noise intensity leads to a spreading of the distribution of the protein concentration values that x can assume. It is only in an *optimal* range of noise values, approximately when the noise intensity is comparable to the potential energy barrier, that the system switches to the other state and remains in the new state: from a biological point of view, the system has chosen the other possible pathway with respect to the one where it was prior to the switch.

To apply this model to the modified version of the LSR paradigm, we have chosen two parameters: one for encoding the logic gate inputs, α, and the other as a control variable to implement a morphable logic gate (in particular, in this work, to switch from the AND to the OR gate and vice versa), γ. The plotted $U(x)$ curves represent the most robust configuration in the limited range of parameters, α and γ, germane to the biological system. Several simulations have been made to exhaustively search (in the parameter space) those parameters that yields the best logic gate performances. For the new version of the LSR paradigm, we obtained (numerically) $\alpha = 6.3$, 9.8, and 13.3 [respectively for (0,0), (0,1)/(1,0), and (1,1)] and $\gamma = 50,36$ to implement the AND and OR gates (respectively).

After applying these α and γ values to Eq. (13), the stochastic differential equation, on the dimensionless interval [0,7000], is integrated by the Euler-Maruyama method. In

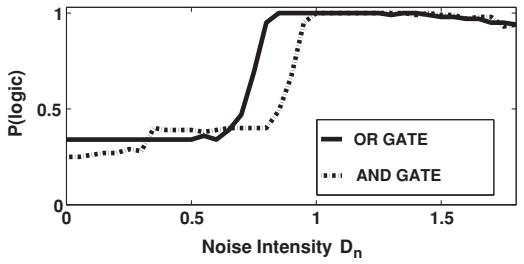

FIG. 4. Performance of logic gates OR and AND, using the modified LSR paradigm, versus the additive noise intensity D_n. α and γ values as in the text.

simulations, it is observed that 7000 is longer than the mean escape time required to switch from the "wrong" to the "correct" (depending on the desired logic outcome) well; this time length also ensures the expected logical output for a large number of trials. To quantify this behavior with respect to noise in this (designed) logic gate we measured its performance as defined as the ratio of success in realizing the desired gate over the total number of attempts; this ratio is the probability $P(\text{logic})$ of realizing the desired gate and is shown (for OR and AND gates) in Fig. 4.

Note that, for each noise value, we have checked the agreement between the simulated logical outputs for all the three data inputs [(0,0),(0,1)/(1,0),(1,1)] and the respective truth table values of the gate under study. If one of the outputs does not realize the desired gate, we mark that as a failure. If, for example, we consider one of the panels in Fig. 3 for each noise value the least robust potential configuration (among the three plotted) will have the highest influence on the performance quality of this considered gate. This procedure is repeated 500 times. The remarkable thing here, then, is that the output conforms to the truth tables in the presence of noise. More explicitly, in a relatively wide window of noise intensity, the system yields logic operations with near certainty, i.e., $P(\text{logic}) \sim 1$. We can conclude that the two gates are robust to noise in the same range of noise and amenable to the design of a morphable logic gate.

Finally, we note that the best performance in the logic gates can be achieved via two possible routes: changing the noise intensity [46,47] or the variation of the parameter values, thereby adjusting the system dynamics to an optimal configuration, so $P(\text{logic}) \sim 1$ as desired; for a nonlinear system this is tantamount (as already noted earlier) to changing the transfer characteristic, thereby "tuning" the noise. In Fig. 5, the gate performance is plotted versus noise intensities and α values (setting $\gamma = 50$ for the AND gate and $\gamma = 36$ for the OR gate). For a fixed value of noise (for example, the one mandated by nature) it is possible to select the "best" α value. It is interesting to note that (for our particular choice of model parameters) if the noise parameter D_n values are in the [0.95,1.35] regime, there is a reasonably large range of α values for which $P(\text{logic}) \sim 1$, as desired.

In a completely analogous way, by setting the output values in the reverse configuration, we can realize NAND and NOR gates in almost the same optimal noise intensity regime as the previous case (e.g., the left well can represent the value 1 for

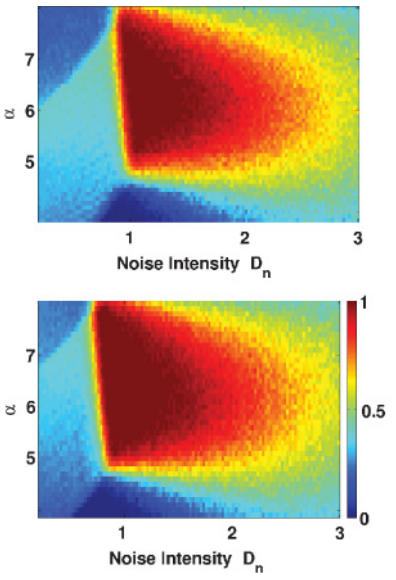

FIG. 5. (Color online) Performance of logic gates AND (top) and OR (bottom) versus noise intensity D_n, and α. γ values as in the text.

output of the NAND/NOR reconfigurable gate, instead of 0 as set previously for the AND/OR gate).

VI. MULTIPLICATIVE NOISE

A complete GRN characterization necessitates extending our model to the case when the system is in presence of an *internal* noise source. With internal noise, we want to define all the random fluctuations that are related to the reactions inside the cell at the gene level; in other words the noise originates, in this case, from the underlying biochemical reactions rather than from external perturbations. In biochemistry, slow reactions such as translation and transcription lead naturally to large noise intensity; their rates are typically small and random fluctuations are consequently more evident [33,48].

It is worth pointing out that simply having an "internal" noise source does not imply that the noise is state dependent (or multiplicative). An obvious example is afforded by a coupled network of nonlinear elements (e.g., a neural network) each one having its own intrinsic noise that is uncorrelated with the noise floors of the other elements in the network. However, when there is a well-defined separation of time scales in the network, or at the onset of a bifurcation when the dynamics can be collapsed onto a single (or a few) variable, the adiabatic elimination process can lead to state-dependent noise in the slow variable (this being the variable that carries all the salient features of the dynamics). Accordingly, in this work we, phenomenologically, introduce multiplicative noise into the dynamics at hand. This is accomplished by considering the Langevin equation [49] corresponding to Eq. (11) and allowing the degradation term, γ, or the transcription term, α, to fluctuate. These two cases will be studied separately but always in presence of an (additive) external noisy background. It means that in our model and simulations, we will deal with simultaneously occurring multiplicative and additive noise terms.

A. Noise in the degradation rate

Now consider the effect of a noise source that alters the degradation rate. We vary this term, allowing the parameter γ in Eq. (11) to fluctuate, i.e., we set $\gamma \to \gamma - D_m\eta(t)$, in presence of a noisy background $D_n\xi(t)$. In this way, we obtain the Langevin equation describing the evolution of the repressor protein concentration, x,

$$\dot{x} = f(x,\alpha,\gamma) + h(x)D_m\eta(t) + D_n\xi(t), \tag{16}$$

where the term $D_n\xi(t)$ has been detailed in Sec. II. The noise term η is a white Gaussian noise with a zero mean and $\langle\eta(t)\eta(t')\rangle = \delta(t-t')$ and intensity D_m. $f(x)$ and $h(x)$ represent two nonlinear functions. To investigate the effects of the additive and multiplicative noise on the genetic regulatory system, we will consider, for simplicity, that $\xi(t)$ and $\eta(t)$ in Eq. (16) are independent of each other, i.e.,

$$\langle\xi(t)\eta(t')\rangle = \langle\eta(t)\xi(t')\rangle = 0. \tag{17}$$

We now apply Eq. (16) to the autoregulatory gene network under study [see Eq. (11)]. We obtain:

$$\begin{aligned}\dot{x} &= \frac{(\alpha-1)x^2 + \sigma_1(\alpha\beta-1)x^4 - \sigma_1\sigma_2x^6}{(\tau+x)(1+x^2+\sigma_1x^4+\sigma_1\sigma_2x^6)} \\ &\quad -\frac{[\gamma - D_m\eta(t)]x}{\tau+x} + \frac{1-\gamma_y x^2}{\tau+x} + D_n\xi(t) \\ &= \frac{(\alpha-1)x^2 + \sigma_1(\alpha\beta-1)x^4 - \sigma_1\sigma_2x^6}{(\tau+x)(1+x^2+\sigma_1x^4+\sigma_1\sigma_2x^6)} \\ &\quad +\frac{1-\gamma x-\gamma_y x^2}{\tau+x} + \frac{D_m\eta(t)x}{\tau+x} + D_n\xi(t),\end{aligned} \tag{18}$$

where

$$\begin{aligned}f(x) &= \frac{(\alpha-1)x^2 + \sigma_1(\alpha\beta-1)x^4 - \sigma_1\sigma_2x^6}{(\tau+x)(1+x^2+\sigma_1x^4+\sigma_1\sigma_2x^6)} \\ &\quad +\frac{1-\gamma x-\gamma_y x^2}{\tau+x}\end{aligned} \tag{19}$$

and

$$h(x) = \frac{x}{\tau+x}. \tag{20}$$

The Fokker-Planck equation [45,50] for the probability density function $P(x,t)$ of being in the state x at time t takes the form, using the Stratonovich prescription,

$$\frac{\partial P(x,t)}{\partial t} = -\frac{\partial}{\partial x}[a(x)P(x,t)] + \frac{1}{2}\frac{\partial^2}{\partial x^2}[b(x)P(x,t)] \tag{21}$$

with the drift and diffusion terms given by

$$\begin{aligned}a(x) &= f(x) + \frac{1}{4}\frac{\partial}{\partial x}b(x) = f(x) + \frac{1}{4}\frac{\partial}{\partial x}\left[D_m^2h(x)^2 + D_n^2\right] \\ &= \frac{(\alpha-1)x^2 + \sigma_1(\alpha\beta-1)x^4 - \sigma_1\sigma_2x^6}{(\tau+x)(1+x^2+\sigma_1x^4+\sigma_1\sigma_2x^6)} \\ &\quad +\frac{1-\gamma x-\gamma_y x^2}{\tau+x} + \frac{1}{4}\frac{\partial}{\partial x}\left[D_m^2\left(\frac{x}{\tau+x}\right)^2 + D_n^2\right]\end{aligned} \tag{22}$$

and

$$b(x) = D_m^2h(x)^2 + D_n^2 = D_m^2\left(\frac{x}{\tau+x}\right)^2 + D_n^2. \tag{23}$$

Equation (21) may be solved in the steady state to obtain the long-time probability density function:

$$P_S(x) = N_{\text{mul\_}\gamma}\exp[-U_g(x)], \tag{24}$$

where $N_{\text{mul\_}\gamma}$ is a normalization term, while the potential $U_g(x)$ takes the form,

$$U_g(x) = -2\int^x \frac{a(y)}{b(y)}dy + \ln b(x). \tag{25}$$

We have checked that, in absence of fluctuations in η (i.e., $D_m = 0$), the results in Sec. V are recovered. The multiplicative noise modifies the drift term $a(x)$ through the presence of the third term in Eq. (22). This means that noise not only influences the dynamics of our biological model but also changes the potential shape configuration: increasing or decreasing the depth of the wells, as well as altering the locations of the fixed points. Moreover, it has been seen [45,51], that multiplicative noise can yield *noise-induced critical behavior* that occurs in addition to the nonlinearity-induced bistability that just exists in the potential shape. All these rich effects, of course, are related to particular parameter values.

In this section, we now proceed as in Sec. V: we plot the bifurcation diagrams in the parameter ranges germane to the biological system; subsequently, we show $U_g(x)$ for the best α and γ values that can give a logic gate performance [$P(\text{logic}) \sim 1$] in a larger area of parameter values (several simulations have been made to exhaustively search the most robust configuration of parameters); finally, we plot the logic gate performance versus the multiplicative noise intensity for fixed additive noise values.

Before starting the whole analysis, we have tried to check the logic gate performance for the best α and γ values obtained in Sec. V. In particular, we wanted to test if the biological system is still robust to the presence of a multiplicative noise source while $\alpha = 6.3$, 9.8, and 13.3 [respectively for (0,0),(0,1)/(1,0),(1,1)] and $\gamma = 50, 36$ (see previous section). We checked the $P(\text{logic})$ versus the additive noise intensity (as in Fig. 4), for different fixed multiplicative noise intensities. The result (not shown) is that the best α and γ values, for the additive noise case, are no longer the best ones in this new condition (i.e., with the inclusion of multiplicative noise) for the implementation of the LSR paradigm. Thus, we are lead to study the logic gate performance versus the multiplicative noise intensity.

In the presence of a random degradation rate, the system shows regions of monostability and bistability as visible in Fig. 6. The left panel represents the bifurcation diagram varying the multiplicative noise intensity, D_m, and α, while γ and D_n are fixed. In the central panel, we vary γ and α, fixing the other two parameters, and, finally, we plot the bifurcation diagram versus D_m and γ.

Figure 6 gives the range where one should, exhaustively, search for the best biological system parameters. In this case, as in Sec. V, α is the parameter used to encode the logic gate inputs, and γ the parameter for switching from the AND to the OR gate. For the new version of the LSR paradigm, we obtained (numerically) $\alpha = 5$, 14.5, and 24 [respectively, for (0,0),(0,1)/(1,0),(1,1)] and $\gamma = 60$, 40 to implement the AND and OR gates (respectively). The potential functions for

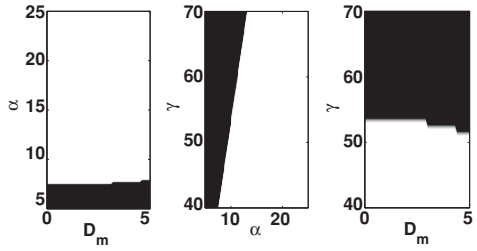

FIG. 6. Bifurcation diagram for $\gamma \to \gamma - D_m\eta(t)$. In the left panel, we varied D_m and α, fixing $\gamma = 40$. In the central panel, we varied α and γ, fixing $D_m = 3$; and, finally, we varied D_m and γ, fixing $\alpha = 10$. In all the three cases we fixed $D_n = 0.5$. The white area represents the bistable region, while the black area represents the monostable region.

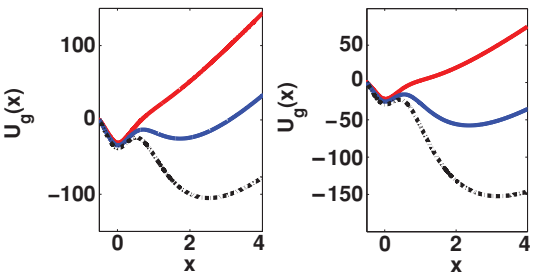

FIG. 7. (Color online) Multiplicative noise. Potential functions for different data inputs for the AND gate (left panels) and the OR gate (right panels), using the modified version of the LSR paradigm (see Sec. IV). The red (upper) curve represents the (0,0) case, the blue (central) curve represents the (0,1)/(1,0) cases, and the black (lower) curve is for the (1,1) case. Values in the accessible parameter range, related to the most robust configuration (see text), have been chosen. In this case the fixed multiplicative noise intensity is $D_m = 3$ and the additive noise intensity $D_n = 0.5$.

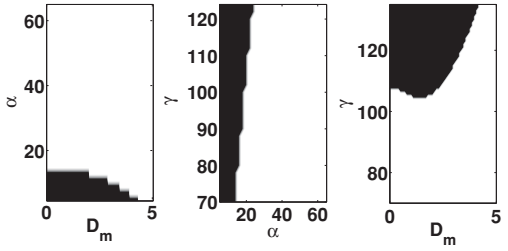

FIG. 9. Bifurcation diagram for $\alpha \to \alpha + D_m\eta(t)$. In the left panel, we varied D_m and α, fixing $\gamma = 71$. In the central panel, we varied α and γ, fixing $D_m = 0.8$; and, finally, we varied D_m and γ, fixing $\alpha = 20$. In all the three cases we fixed $D_n = 0.5$. The white area represents the bistable region, while the black area represents the monostable region.

AND and OR gates for different data inputs are presented in Fig. 7.

Finally, the AND and OR performances are plotted (Fig. 8) versus the noise intensity D_m. All the parameter values in Fig. 8 are the same as Fig. 7. Again we have tested that, in this new configuration, the dimensionless time interval [0,7000] is long enough to let the system switch from the "wrong" to the "correct" well; the simulations in this case follow the same method explained in Sec. V. Comparing the results in Fig. 8 with those in Fig. 4, we see, clearly, the large increment in the optimal window of noise where $P(\text{logic}) \sim 1$, the estimated range is $D_m = [2.7,3.5]$. This is due to the potential shape that changes with D_m for the multiplicative noise case: in the range where the performance is around 1, D_m makes the potential function $U_g(x)$ asymmetric in order to better perform the AND or OR gates. The LSR in bacteriophage λ is robustly realized for high noise intensities of D_m, because the potential barrier of the "wrong" well assumes larger values than in the additive-noise-only case. The different panels in Fig. 8 show that it is possible to implement LSR also in a broad additive noise intensity range.

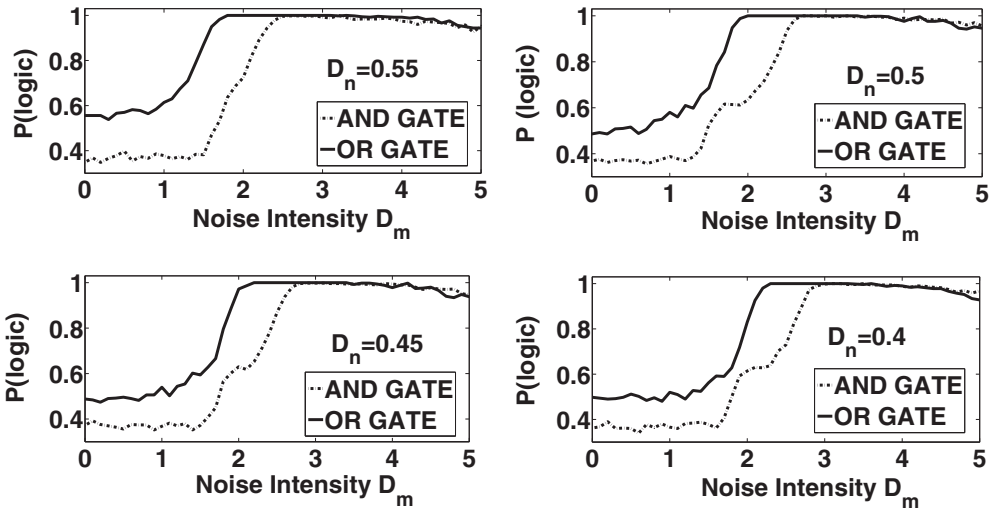

FIG. 8. Performance of logic gates AND and OR versus the multiplicative noise intensity D_m; $\alpha = 5$, 14.5, and 24 for the three input sets, $\gamma = 60$, 40 (to implement the AND and OR gates, respectively), for different fixed D_n values.

B. Noise in the transcription rate

In order to simulate the stochastic effects of the gene transcription regulation, we consider the perturbation of the parameter α. As we saw in Sec. V, α is related to the transcription rate, and we set it as $\alpha \to \alpha + D_m\eta(t)$ in the presence of a noisy term $D_m\eta(t)$.

In this case, Eq. (16) will have the following form for our autoregulatory gene network:

$$\dot{x} = \frac{(\alpha + D_m\eta(t) - 1)x^2 + \sigma_1\{[\alpha + D_m\eta(t)]\beta - 1\}x^4 - \sigma_1\sigma_2 x^6}{(\tau + x)(1 + x^2 + \sigma_1 x^4 + \sigma_1\sigma_2 x^6)} + \frac{1 - \gamma x - \gamma_y x^2}{\tau + x} + D_n\xi(t)$$

$$= \frac{(\alpha - 1)x^2 + \sigma_1(\alpha\beta - 1)x^4 - \sigma_1\sigma_2 x^6}{(\tau + x)(1 + x^2 + \sigma_1 x^4 + \sigma_1\sigma_2 x^6)} + \frac{1 - \gamma x - \gamma_y x^2}{\tau + x} + \frac{D_m\eta(t)(x^2 + \sigma_1\beta x^4)}{(\tau + x)(1 + x^2 + \sigma_1 x^4 + \sigma_1\sigma_2 x^6)} + D_n\xi(t), \quad (26)$$

where $f(x)$ is the same as in Eq. (19), while $h(x)$ is

$$h(x) = \frac{x^2 + \sigma_1\beta x^4}{(\tau + x)(1 + x^2 + \sigma_1 x^4 + \sigma_1\sigma_2 x^6)}. \quad (27)$$

For a given α value, the steady-state probability distribution $P(x,t)$ can be obtained by transforming Eq. (26) in a nonlinear Fokker-Planck equation [45,50], where x is the protein concentration. Setting Eq. (21) equal to 0, we obtain the longtime probability density function:

$$P_S(x) = N_{\text{mul}\_\alpha} \exp\left[-U_a(x)\right], \quad (28)$$

where N_{mul_α} is a normalization term, while the potential $U_a(x)$ takes the form,

$$U_a(x) = -2\int^x \frac{a(y)}{b(y)}dy + \ln b(x). \quad (29)$$

Because we are dealing with a noisy α value, the terms $a(x)$ and $b(x)$ will have the form:

$$a(x) = f(x) + \frac{1}{4}\frac{\partial}{\partial x}b(x) = f(x) + \frac{1}{4}\frac{\partial}{\partial x}\left[D_m^2 h(x)^2 + D_n^2\right]$$

$$= \frac{(\alpha - 1)x^2 + \sigma_1(\alpha\beta - 1)x^4 - \sigma_1\sigma_2 x^6}{(\tau + x)(1 + x^2 + \sigma_1 x^4 + \sigma_1\sigma_2 x^6)} + \frac{1 - \gamma x - \gamma_y x^2}{\tau + x}$$

$$+ \frac{1}{4}\frac{\partial}{\partial x}\left\{D_m^2\left[\frac{x^2 + \sigma_1\beta x^4}{(\tau + x)(1 + x^2 + \sigma_1 x^4 + \sigma_1\sigma_2 x^6)}\right]^2 + D_n^2\right\} \quad (30)$$

and

$$b(x) = D_m^2\left[\frac{x^2 + \sigma_1\beta x^4}{(\tau + x)(1 + x^2 + \sigma_1 x^4 + \sigma_1\sigma_2 x^6)}\right]^2 + D_n^2. \quad (31)$$

Before plotting the performance of LSR, we exhaustively searched for the best α and γ values that can realize the AND and OR gates for this particular noisy condition. In Fig. 9, we show the bifurcation diagrams and particularly the parameter ranges where it is possible to best perform the new version of the LSR paradigm. The obtained best values are $\alpha = 20, 42.4$, and 64.8 (for the input sets), and $\gamma = 122, 71$ to implement the AND and OR gates. The resultant potential functions U_a have being plotted in Fig. 10 for a particular multiplicative noise value $D_m = 0.8$.

It is possible to notice how the left well is always smaller than the right well. The consequence of this behavior is evident in the performance graphs (see Fig. 11): $P(\text{OR}) \sim 1$ in a larger range than $P(\text{AND})$. It means that the possibility to implement a reliable logic gate in a large interval, mostly depend on the possibility to realize an AND gate in presence of noise. In Fig. 11, the AND and OR performances are plotted versus the noise intensity D_m. Again we have tested that, in this new configuration, the dimensionless time interval [0, 7000] is long enough to let the system reach the correct well. The procedure for this case is the same used in all the manuscript and it has been repeated 500 times.

In contrast to the previous Sec. VI A, we found a difficulty in performing the two logic gates with $P(\text{logic}) \sim 1$ for a large range of D_m [in this case $P(\text{logic}) \sim 1$ for $D_m = [0.75, 0.95]$ and $D_n = 1$]. This is due to the high nonlinearity of the $h(x)$ term in Eq. (27) that has resulted in a new bistable potential. Moreover, simulations with $D_n \sim 0.5$ were not showing a $P(\text{logic}) \sim 1$: this additive noise intensity was not enough to let the system reach the correct well. It is manly due to the potential function: it considerably changes over the multiplicative noise increment. Following these results, we simulated the performance for different and fixed D_n values, and we obtained that the logic gate performance was improving in presence of an higher additive noise intensity: $D_n \sim 1$ (see Fig. 11). The reported values are still in a realistic biological range.

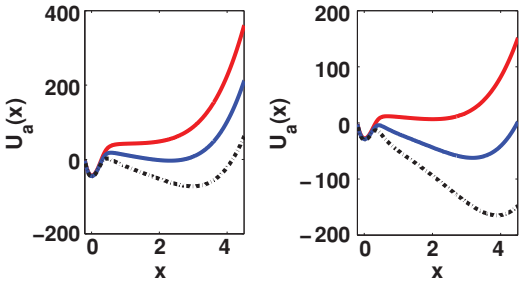

FIG. 10. (Color online) Potential functions for different data inputs for the AND gate (left panels) and the OR gate (right panels), using the modified version of LSR paradigm (see Sec. IV). The red (upper) curve represents the (0,0) case, the blue (central) curve represents the (0,1)/(1,0) cases, and the black (lower) curve is for (1,1) case. Values in the accessible parameter range, related to the most robust configuration (see text), have been chosen. In this case the fixed multiplicative noise intensity is $D_m = 0.8$ and the additive noise intensity $D_m = 0.5$.

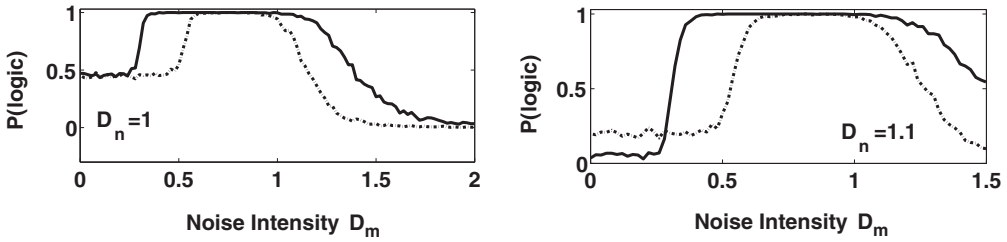

FIG. 11. Performance of logic gates OR (the straight line in each panel) and AND (the dashed line in each panel) using the modified LSR paradigm versus the multipicative noise intensity D_m; α and γ values as in the text, for different D_n values.

The LSR in bacteriophage λ is robustly realized for noise intensities of D_m lower than the previous case (see Sec. VI A): the change in the multiplicative noise intensity has a great influence in the shape of the potential function. The different panels in Fig. 11 show that it is possible to implement LSR not only in an optimal range of D_m values but also in a broad range of additive noise values, D_n.

VII. CONCLUSION

To summarize, we have implemented a new version of LSR in a GRN, specifically the bacteriophage λ. We have shown that the resultant computing device is able to work as an AND or OR gate interchangeably in the presence of noise. In a completely analogous way, by setting the output values in the reverse configuration, we can realize NAND and NOR gates in almost the same optimal noise intensity regime as the previous case (e.g., the left well can represent the 1 for output of the NAND/NOR reconfigurable gate, instead of 0 as set previously for the AND/OR gate). Noise is critical for the existence and operation of the gates. We have computed the gate "performance" as a function of noise intensity and shown that the biological system output is the logical combination of the two data inputs for a range of noise intensities, and the GRN phage λ can switch from the AND to OR gate as desired; this switching can be accomplished, for a fixed noise level, by adjusting other *deterministic* system parameters.

In this work we, first, investigated how the presence of an *external* noise source acts on the autoregulatory gene network under consideration. In this case we modeled the fluctuations through an additive noise term. Thereafter, we studied *internal* noise as a source that affects the degradation and the transcription rates. To accomplish this, we introduced a multiplicative noise term setting, in separate cases, $\gamma \to \gamma - D_m\eta(t)$ and $\alpha \to \alpha + D_m\eta(t)$, respectively.

LSR on a GRN, that has the capability of being reconfigured, could be combined, in the near future, with other logic modules (done by different sets of input/output signals) to increase the computational power and functionality of an engineered GRN. Recently, several experiments have demonstrated the possibility of using external inducers to control gene regulation [7,13]. For example, gene expression, under the control of the promoter with Olac binding sites, can be repressed by adding a gene that produces the LacI protein, which can in turn be inactivated by IPTG (isopropyl-β-D-thiogalactopyranoside) quickly [7]. IPTG induction can be applied with accurate control by using customized microfluidics devices [13], thereby establishing a temporal control over the GRN. Such networks may allow predictable and robust control in fluctuating cellular environments and thereby have a significant impact in the design of synthetic biological systems such as recently created bacterial cells controlled by chemically synthesized genomes [52].

ACKNOWLEDGMENTS

We gratefully acknowledge support from the Office of Naval Research under Grants No. N000140211019 and No. N0000148WX20330AA. A.R.B. acknowledges fruitful conversations with Professor Bart Kosko.

[1] S. Mukherji and A. van Oudenaarden, Nat. Rev. Genet. **10**, 859 (2009).
[2] M. Kaern, W. Blake, and J. J. Collins, Annu. Rev. Biomed. Eng. **5**, 179 (2003).
[3] J. Hasty, D. McMillen, and J. J. Collins, Nature (London) **420**, 224 (2002).
[4] H. H. McAdams and L. Shapiro, Science **269**, 650 (1995).
[5] T. S. Gardner, C. R. Cantor, and J. J. Collins, Nature (London) **403**, 339 (2000).
[6] S. S. Shen-Orr, R. Milo, S. Mangan, and U. Alon, Nat. Genet. **31**, 64 (2002).
[7] T. Ellis, X. Wang, and J. J. Collins, Nat. Biotechnol. **27**, 465 (2009).
[8] B. Canton, A. Labno, and D. Endy, Nat. Biotechnol. **26**, 787 (2008).
[9] C. M. Ajo-Franklin, D. A. Drubin, J. A. Eskin, E. P. Gee, D. Landgraf, I. Philips, and P. A. Silver, Genes Dev. **21**, 2271 (2007).
[10] D. Nevozhaya, R. M. Adamsa, K. F. Murphy, K. Josićc, and G. Balázsi, Proc. Natl. Acad. Sci. USA **106**, 5123 (2009).
[11] J. Cherry and F. Adler, J. Theor. Biol. **203**, 117 (2000).
[12] M. B. Elowitz and S. Leibler, Nature (London) **403**, 335 (2000).
[13] J. Stricker, S. Cookson, M. R. Bennet, W. H. Mather, L. S. Tsimring, and J. Hasty, Nature (London) **456**, 27 (2008).
[14] D. Karig and R. Weiss, Biotechnol. Bioeng. **89**, 709 (2005).
[15] G. J. Nistala, K. Wu, C. V. Rao, and K. D. Bhalerao, J. Biol. Eng. **4**, 4 (2010).

[16] W. Weber, B. P. Kramer, and M. Fussenegger, Biotechnol. Bioeng. **98**, 894 (2007).
[17] C. J. Bashor, N. C. Helman, S. Yan, and W. A. Lim, Science **319**, 1539 (2008).
[18] S. Hooshangi, S. Thiberge, and R. Weiss, Proc. Natl. Acad. Sci. USA **102**, 3581 (2005).
[19] A. Becskei and L. Serrano, Nature (London) **405**, 590 (2000).
[20] A. Eldar and M. B. Elowitz, Nature (London) **467**, 167 (2010).
[21] L. Gammaitoni, P. Hänggi, P. Jung, and F. Marchesoni, Rev. Mod. Phys. **70**, 223 (1998).
[22] A. R. Bulsara and L. Gammaitoni, Phys. Today **49**, 39 (1996).
[23] K. Wiesenfeld and F. Moss, Nature (London) **373**, 33 (1995).
[24] M. Thattai and A. van Oudenaarden, Proc. Natl. Acad. Sci. USA **98**, 8614 (2001).
[25] V. Shahrezaei, J. F. Ollivier, and P. S. Swain, Mol. Syst. Biol. **4**, 196 (2008).
[26] K. Murali, S. Sinha, W. L. Ditto, and A. R. Bulsara, Phys. Rev. Lett. **102**, 104101 (2009).
[27] M. Ptashne, *A Genetic Switch: Phage λ and Higher Organisms*, 2nd ed. (Cell Press & Blackwell Scientific, Cambridge, MA, 1992).
[28] A. D. Johnson, A. R. Poteete, G. Lauer, R. T. Sauer, G. K. Ackers, and M. Ptashne, Nature **294**, 217 (1981).
[29] J. Hasty, J. Pradines, M. Dolnik, and J. J. Collins, Proc. Natl. Acad. Sci. USA **97**, 2075 (2000).
[30] D. Guerro, A. Bulsara, W. Ditto, S. Sinha, K. Murali, and P. Mohanty, Nano Lett. **10**, 1168 (2010).
[31] A. R. Bulsara, A. Dari, W. L. Ditto, K. Murali, and S. Sinha, Chem. Phys. **375**, 424 (2010).
[32] B. Lewin, *Genes*, Vol. VI (Oxford University Press, Oxford, UK, 1997).
[33] C. V. Rao, D. M. Wolf, and A. P. Arkin, Nature (London) **420**, 231 (2002).
[34] J. Hasty, F. Isaacs, M. Dolnik, D. McMillen, and J. J. Collins, Chaos **11**, 207 (2001).
[35] A. Becskei, B. Sŕaphin, and L. Serrano, EMBO J. **20**, 2528 (2001).
[36] F. J. Isaacs, J. Hasty, C. R. Cantor, and J. J. Collins, Proc. Natl. Acad. Sci. USA **100**, 7714 (2003).
[37] R. Calendar, ed., *The Bacteriophages* (Oxford University Press, New York, 2005).
[38] B. J. Meyer, R. Maurer, and M. Ptashne, J. Mol. Biol. **139**, 163 (1980).
[39] G. K. Ackers, A. D. Johnson, and M. A. Shea, Proc. Natl. Acad. Sci. USA **79**, 1129 (1982).
[40] M. Ptashne, A. Jeffrey, A. D. Johnson, R. Maurer, B. J. Meyer, C. O. Pabo, T. M. Roberts, and R. T. Sauer, Cell **19**, 1 (1980).
[41] A. D. Johnson, C. O. Pabo, and R. T. Sauer, Methods Enzymol. **65**, 839 (1980).
[42] M. Morelli, P. ten Wolde, and R. Allen, Proc. Nat. Acad. Sci. USA **106**, 8101 (2009).
[43] M. B. Elowitz, A. J. Levine, E. D. Siggia, and P. S. Swain, Science **297**, 1183 (2002).
[44] H. H. McAdams and A. Arkin, Proc. Natl. Acad. Sci. USA **94**, 814 (1997).
[45] H. Risken, *The Fokker-Planck Equation* (Springer-Verlag, Berlin, 1984).
[46] T. Lu, M. Ferry, R. Weiss, and J. Hasty, Phys. Biol. **5**, 036006 (2008).
[47] K. F. Murphy, R. M. Adams, X. Wang, G. Balázsi, and J. J. Collins, Nucl. Acids Res. **38**, 2712 (2010).
[48] A. M. Kierzek, J. Zaim, and P. Zielenkiewicz, J. Biol. Chem. **16**, 8165 (2001).
[49] C. W. Gardiner, *Handbook of Stochastic Methods* (Springer-Verlag, Berlin, 1983).
[50] N. S. Goel and N. Ritcher-Dyn, *Stochastic Models in Biology* (The Blackburn Press, New Jersey, 1974).
[51] A. R. Bulsara, R. D. Boss, and E. W. Jacobs, Biol. Cybern. **61**, 211 (1989).
[52] D. G. Gibson *et al*., Sci. Express **329**, 52 (2010).